CHAPTER 7

MICROHARDNESS ANISOTROPY OF CALCIUM MOLYBDATE SINGLE CRYSTALS

Contents | Pages

7.1 INTRODUCTION

Hardness is an important solid state property (1) which is commonly studied to determine the mechanical strength and other properties of materials. Point indentation techniques such as Vickers pyramid test, Hertz test and Knoop test have been commonly used by several investigators (2-6) to study glide, deformation anisotropy, cracks, etc. in various crystals. Nonetheless, indentation is carried out using sharp indenters such as cones and pyramids, because of the geometrical similarity of their residual impression. With such geometry, the contact pressure is independent of indent size, and thus offers a convenient measure of hardness (7). The Vickers test is one of the most reliable methods for hardness measurements since it is independent of pre-existing surface flaw conditions (8) and is far less time-consuming (9) and has the potential of yielding a better statistical average with far fewer indentations. The literature survey reveals that the study of hardness has not so often been carried out on non-cubic crystals. Unlike quenched and annealed alkali halides (10,11), other crystals have hardly been investigated for their hardness. Also, practically no information is available on the micromechanical behaviour of calcium molybdate. The

nature of this bulk-grown material makes Vickers microhardness a favourable parameter of study. Hence a systematic study on the hardness characteristics of these crystals was thought worthwhile to be undertaken at room temperature, so also to establish the effect of quenching and annealing on their microhardness.

7.2 EXPERIMENTAL

The grown crystals of $CaMoO_4$ having smooth and plane surfaces were selected, after examining them under the "Epignost" optical microscope. Static indentations on the as-grown smooth (011), and also the cleavage (001) planes, in air, at room temperature (30°C) were made by a standard pyramidal diamond indenter, using Vickers microhardness tester MO 6027 manufactured by Vickers Ltd., U.K. The loads were applied in steps from 10 to 100 g. over a fixed interval of time, viz., 15 sec. The loading time was kept fixed because the hardness value was found to be independent of this factor in our crystals, though in certain cases (12) the two may be mutually dependent. The indents were made at different sites so that the distance between two successive marks of indentation was much greater than the indent diagonal length, thus ensuring surface effects to be independent

of one another. From the mean value of the diagonals of the square indentation marks 'd', measured using a filar micrometer (least count 0.001 cm) of the Vickers projection metallurgical microscope, the Vickers hardness number, VHN, was determined using the relation (13)

$$VHN = 1.854\ P/d^2 \quad kg.\ mm^{-2} \qquad (7.1)$$

where P (in kg) is the applied load and d (in mm) is the mean diagonal length of Vickers impression, measured after unloading. Necessary precautions in mounting the samples were taken in order to minimize error due to misorientation of the experimental crystal surface with respect to the indenter. The length of the cracks developed at the edges of the indentation marks were also measured.

Further, some of the grown crystals were heated at 525, 650 and 775^{o}C i.e. well below the melting point (1450^{o}C), each for a period of two hours and subjected to quenching by suddenly withdrawing them from the furnace and immersing them into cold water. Another set of crystals examined were those annealed in the air atmosphere; this was accomplished by heating them at 525, 650 and 775^{o}C respectively, each for about

five hours, and then to prevent introduction of fresh dislocations, the samples were slowly brought down to room temperature by normal temperature control. For these quenched and annealed crystals also, indentation tests were conveniently performed on the as-grown (011) planes and the VHN values were obtained using the equation (7.1), as a function of the applied load with different quenching and annealing temperatures in the range 30-775^{o}C.

7.3 RESULTS AND DISCUSSION

7.3.1 Vickers microhardness

The cartesian graphs of d^2 versus P for measurements at room temperature (303 K and relative humidity 40 %) are shown in Fig. 7.1 for (011) and (001) planes. Obviously, d^2 is directly proportional to P, thus supporting the use of equation (7.1) to compute VHN. The systematic variation of microhardness of the specimen with load is shown in Figs. 7.2 (a and b) for the two planes, revealing that the variation of VHN is, contrary to the theoretical expectation, not uniform throughout. For immediate comparison of the two cases, they have been plotted together also as shown in Fig. 7.3. For both the planes, it is seen that the VHN increases with load, reaching a sharp maximum at 50 g and finally

reaches a saturation, steady value, beyond about 70 g. The absolute values of the constant VHN obtained at a load of 80 g are 469.50 kg. mm^{-2} and 365.87 kg. mm^{-2} for (011) and (001) planes respectively. A cursory remark can be made about the relative hardness value in the higher load region for the two observed planes. The VHN in the case of (011) plane is greater than that for the (001) plane by 28.32 %. This points to the fact the surfaces are softer along the cleaved planes. In $CaMoO_4$ structure the cleavage along (001) plane easily separates MoO_4 tetrahedra from Ca atoms, whereas the tetrahedral packing of atoms on the (011) plane is relatively harder to be ruptured.

The region for the indenting loads up to 80 g on the VHN versus load curves (Fig. 7.3) constitutes what can be termed as the microhardness region, according to the concept of Onitsch (14). In this region, the load P and the corresponding diagonal length d of the indentation mark are related as

$$P = ad^n \qquad (7.2)$$

where 'a' and 'n' are constants for a given material. Kick's (15) analysis of hardness has postulated a

constant value of 'n' to be equal to 2 for all indenters. This is further supported by Schulz and Hanemann (16). However, Kick's law represented by equation (7.2) has not received wide acceptance on account of the fact that 'n' usually has a value less than 2, especially in the region of low load hardness. Saraf (17) obtained two different values of 'n' for higher and lower load regions in the case of baryte crystals. In our case, however, the values of 'n' at room temperature ($30^{o}C$) for (011) and (001) planes are computed as 2.295 and 2.17 respectively, using the least square method. These values reflect upon the fact that the hardness is both load-sensitive and anisotropic.

7.3.2 Quenched and annealed hardness

Now, with regard to the quenched and annealed microhardness, determined as mentioned in section 7.2, the variation of the VHN with applied load are graphically illustrated in Figs. 7.4 and 7.5. One observes that

(i) The VHN shows similar features of variation in approximately the same load ranges, though the actual values of VHN are temperature dependent.

(ii) For a given load, the VHN markedly increases

with increase in the quenching temperature and markedly decreases with increase in the annealing temperature.

One is inclined to believe that the content and configuration of dislocations produced on quenching, as well as the point defects retained, do influence the magnitude of VHN, as observed. It is noteworthy that each of the curves in Figs. 7.4 and 7.5 for quenched and annealed single crystals consists of three clearly recognizable portions : AB (linear part, up to 20 g), BB'C (non-linear part, between 20 g and 80 g) and CD (linear saturated part, above 80 g), corresponding to low-load region (LLR), intermediate-load region (ILR) and high-load region (HLR), respectively. The three regions suggest different prominent factors operating in different ranges of the applied load. The general behaviour of microhardness with load can, however, be quantitatively understood on the basis of the depth of penetration of the indenter. In LLR, the indenter penetrates only the surface layers and so the effect is shown sharply and proportionately at these loads. The penetration depth increases with applied loads and the overall effect gets combined due to surface and inner layers. This complex effect seems to be

responsible for the non-linear portion of the plot (ILR). Finally, after a certain depth of penetration, the effect of inner layers becomes more prominent as compared to the surface layers and so no variation is observed in the values of VHN with respect to load, thus leading to the linearsaturated region (HLR) on the experimental curves.

The microhardness of the crystals under study was measured up to a quenching temperature of 775°C. A plausible, empirical, relation between the quenched hardness and the temperature could be successfully evolved by plotting log $\bar{H}T_Q$ against log T_Q as shown in Fig.7.6, where $\bar{H}$ is the average microhardness in HLR and T_Q is the quenching temperature. The straight-line curve implies, quantitatively, the relation

$$\log \bar{H}T_Q = m_Q \log T_Q + \log Y \qquad (7.3)$$

where m_Q is the slope and log Y is the intercept on the axis of log $\bar{H}T_Q$ when log T_Q is zero. Further, one obtains

$$\bar{H}T_Q^{1-m_Q} = \bar{H}T^k = C = \text{Constant} \qquad (7.4)$$

where the exponent $k = 1 - m_Q$.

It may be mentioned that similar relation holds good for the air-annealed samples too, that is

$$\bar{H}T_A^{1-m_A} = \bar{H}T^k = C = \text{Constant} \qquad (7.5)$$

Figures 7.6 and 7.7 show the variation of log $(\bar{H}T_Q)$ versus log (T_Q), and log $(\bar{H}T_A)$ versus log (T_A), where the subscript Q refers to quenching and A refers to annealing process. Again, the two straight lines of Figs. 7.6 and 7.7 have been plotted in Fig. 7.8. The two straight line graphs in Fig. 7.8 yield $m_Q = 1.28$ and $m_A = 0.77$. Substituting these values in equations (7.4) and (7.5) gives

$$\bar{H}T_Q^{-0.28} = \text{Constant}$$

and

$$\bar{H}T_A^{0.23} = \text{Constant}$$

The fact that the exponent of temperature is negative for quenched samples and positive for the annealed samples indicates (18) that the load-independent hardness increases with the increase in quenching temperature and diminishes with the increase in annealing temperature.

7.3.3 Crack propagation

While carrying out these studies we have also tried to follow the variation and nature of cracks developed around the Vickers indentation impressions. Here, both the planes, viz. (011) and (001), upon indentation, show sharp indentation marks accompanied by cracks around them. The crystal surface is observed to be chipped-off around the indentation marks at medium and higher load values; the chipping-off occurs non-uniformly from the sides of the indentation marks, depending on the applied load. The observed variation of crack length at different indentation dwell periods with the applied load has been graphically plotted in Fig. 7.9. From this data, we have determined the variation of crack velocity with respect to the applied load which is graphically shown in Fig. 7.10.

Our understanding of events occuring in the deformed zone is very meagre. However, the following observations are noteworthy :

(i) The variation of crack length versus load with the dwell time as a parameter depicted in Fig. 7.9 is reasonably linear.

(ii) It can be inferred from Fig. 7.10 that the

crack velocity remains constant beyond 80 g load which may be due to non-extension of radial cracks beneath the deformed zone.

The indented planes show sharp square indentation marks accompanied by interesting crack patterns around them as shown in Figs. 7.11 (a, b and c). During initial loading the sharp indenter induces a zone of irreversible deformation about the contact point, the size of this zone increases with load, as suggested by Lawn and Swain (19). At some critical indenter load a crack suddenly initiates below the contact point, where the stress concentration is greatest. This crack, commonly termed as median vent, lies on a plane of symmetry in the applied field, the specific orientation of which depends on such factors as indenter geometry and crystal anisotropy. Increasing the load causes further, stable, extension of the median vent. On the other hand, during initial unloading the median vent begins to close and consequently, sideways-extending cracks, termed as lateral vents, lc, begin to appear on the surface. On complete unloading, lateral vents continue to extend, and may cause material chipping. These events can be inferred from Fig. 7.11(a) corresponding to as low loads as 40 g. In situations where the

system is not overloaded (using about 60 g load) both radial and lateral (rc and lc) cracks have been observed to form (Fig. 7.11(b)) during unloading. Under these conditions the radial cracks, rc, are not well-developed and are mainly confined to the specimen surface. These cracks seem to emanate from the corners of the indentation and do not extend beneath the deformed zone. They are similar to the so-called Palmqvist cracks observed in cemented carbides by Ogilvy et al (20). The radial cracks formed at low indenter loads are probably the result of the unloading residual stresses. Hagan and Swain (21) also found similar cracks around inelastic indentations with small spheres.

The mechanism of initiation and propagation of the lateral cracks is less well-understood; the lateral cracks are, however, thought tc start from the similarly favourable surface-flaws at the elastic--plastic boundary and propagate by the rather high tensile unloading stresses (22-25). These stresses are produced by the inability of the material to recover completely, elastically, in the presence of the localised plastic flow. Ogilvy et al (20) have suggested that some shear failure processes in the deformed zone

may be responsible for the formation of the lateral cracks. The observations of Hagan and Swain (21) confirm the finding of Peter (26) about the inhomogeneous shear deformation beneath the indentation and also suggest that the interaction of these shear deformation flow lines is responsible for the nucleation of the median (radial)cracks, whilst the over-strained atomic bonds on the shear bands appear to be nuclei for the lateral cracks.

Further, along with the radial and lateral cracks, annuli or band of cracks, CZ, reflecting the symmetry of the indenter are observed within the surface of the plastic indents. The band of cracks extend into the indent from the edge and is always terminated by a zone cf with little or no cracking as exhibited in Fig. 7.11(b). These cracks could be the intersections of the flow line "rossettes" with the specimen surface (21). These cracks would probably arise from the nature of the elastic surface stresses during indentation. These stresses are greatly modified by frictional effects from either the indenter-sample roughness or the mis-match of elastic properties of the two materials in contact (27).

As the load is increased, (say upto 100 g) these shallow cracks are absorbed into the contact area and a bunch of new cracks are formed at the new contact, resulting into material chipping-off as shown in Fig. 7.11(c) which is an early stage of crushing and powdering of the crystalline matter. This clearly manifests the interaction of heavily worked flow lines forming a tangled mesh beneath and around the deforming indenter.

7.4 CONCLUSIONS

1. The softness of atomic packing along the crystallographic cleavage direction has been indirectly established.
2. The Vickers hardness number increases sharply with load in the lower load region (LLR; $\leqslant$ 20 g) reaching a maximum, then distinctly decreases in the intermediate-load region (ILR; 20-80 g), and ultimately becomes constant in the higher-load region (HLR; $>$ 80 g).
3. In the higher load region, the Vickers microhardness increases with increase in the quenching temperature and decrease with increase in the annealing temperature. The generic relation $\bar{H}T^{k}$ = constant holds good for the treated samples.

4. The crack velocity tends to increase with the applied load, reaching saturation around 80 g.

REFERENCES

1. H. Buckle. (1959)
Met. Rev., 4, 49.

2. C. A. Brookes and P. Green. (1973)
Nature, 246, 119.

3. C. A. Brookes and B. Moxley. (1975)
J. Phys. E., 8, 456.

4. E. H. L. J. Dekker and G. D. Rieck. (1974)
J. Mater. Sci., 9, 1839.

5. Y. Kumashiro, A. Itoh, T. Kinoshita and
M. Sobajima. (1977)
J. Mater. Sci., 12, 595.

6. S. K. Arora, T. Abraham, G. S. T. Rao
and R. S. Godbole.(1982)
J. Mater. Sci., 17, 2825.

7. B. R. Lawn and R. Wilshaw. (1975)
J. Mater. Sci., 10, 1049.

8. T. Haranoh, H. Ishikawa, N. Shinkai
and M. Mizuhashi. (1982)
J. Mater. Sci., 17, 1493.

9. W. J. Weber, H. J. Matzke and J. L. Routbort.
(1984)
J. Mater. Sci., 19, 2533.

10. I. Kishsh and I. Sharkezi. (1971)
Sov. Phys. Crystallogr., 16, 827.

11. R. S. Chaure and R. N. Shrivastava. (1982)
Indian J. Pure and Appl. Phys., 20, 40.

12. A. G. Atkins, A. Silverio and D. Tabor. (1966)
J. Inst. Metals, 94, 369.

13. B. W. Mott. (1966)
"Microindentation Hardness Testing"
(Butterworths, London) 9.

14. E. M. Onitsch. (1947)
Mikroscopie, 2, 131.

15. F. Kick. (1885)
"Das Gesetzder, Proportionalen winderstande
and science anwendung" Leipzig Felix (ed.).

16. F. Schulz and H. Hanemann. (1941)
Z. Ketallk, 33, 124.

17. C. L. Saraf. (1972)
"Optical study of natural and synthetic
beryte crystals".
Ph.D. thesis, M. S. University of Baroda,
Baroda.

18. J. R. Pandya, L. J. Bhagia and
A. J. Shah.(1983)
Bull. Mater. Sci., 5, 79.

19. B. R. Lawn and M. S. Swain. (1975)
J. Mater. Sci., 10, 113.

20. I. M. Ogilvy, C. M. Perrot and
J. W. Suiter. (1977)
Wear, 43, 239.

21. J. T. Hagan and M. V. Swain. (1978)
J. Phys. D. : Appl. Phys., 11, 2091.

22. M. V. Swain and J. T. Hagan. (1976)
J. Phys. D : Appl. Phys., 9, 2201.

23. K. L. Johnson. (1968)
"Engineering Plasticity".
(London : Cambridge UP), 341.

24. K. J. Johnson. (1970)
J.Mech. Phys., 18, 115.

25. C. J. Studman and J. E. Field. (1976)
J. Phys. D. : Appl. Phys., 9, 857.

26. K. W. Peter. (1970)
J. Non. Cryst. Solids, 5, 103.

27. K. L. Johnson, J. J. O'Connar and
A. C. Woodward. (1973)
Proc. Roy. Soc., A 334, 95.

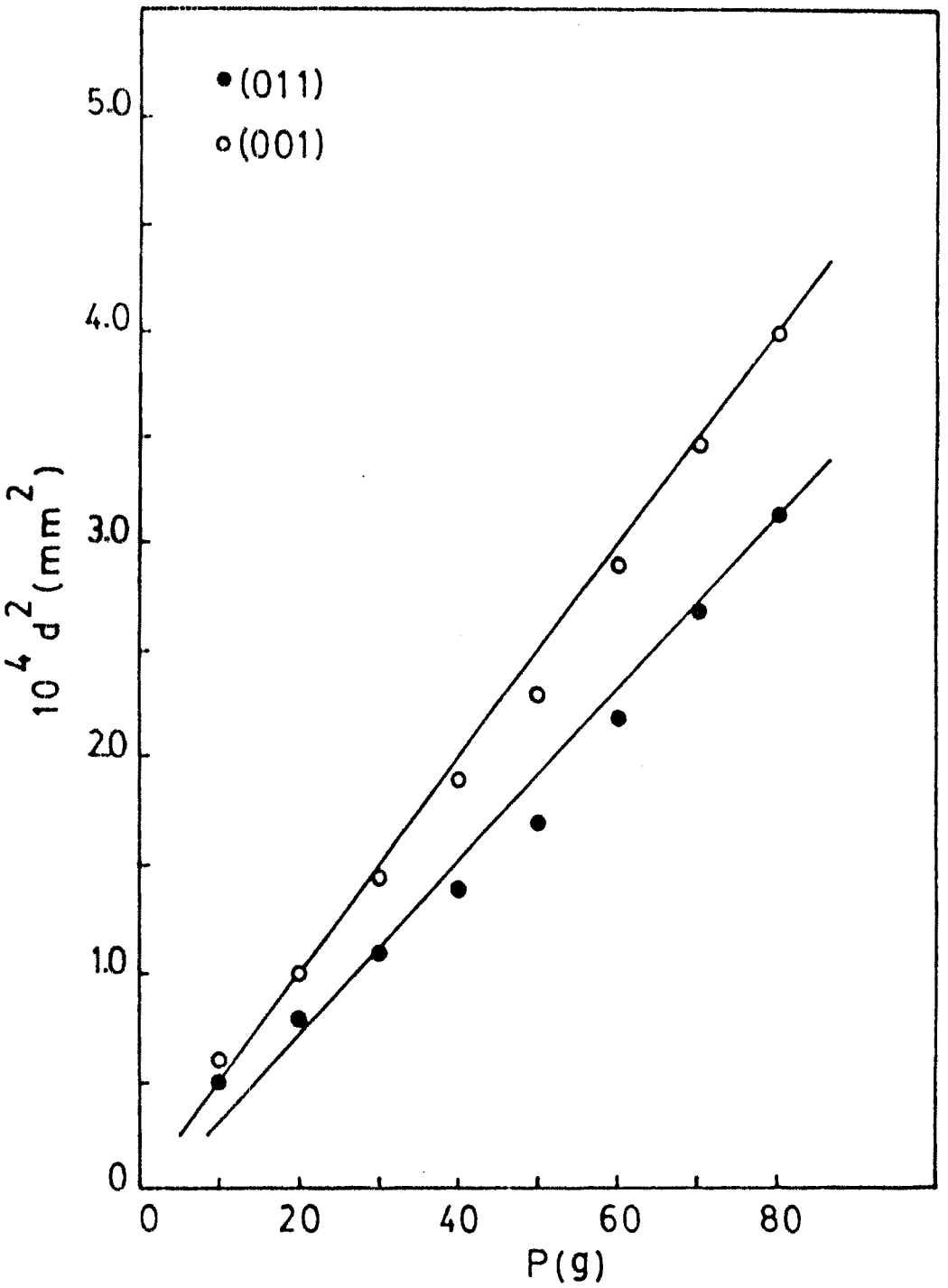

Fig. 7.1 Graphical plot of d^2 against P for (011) and (001) planes at room temperature.

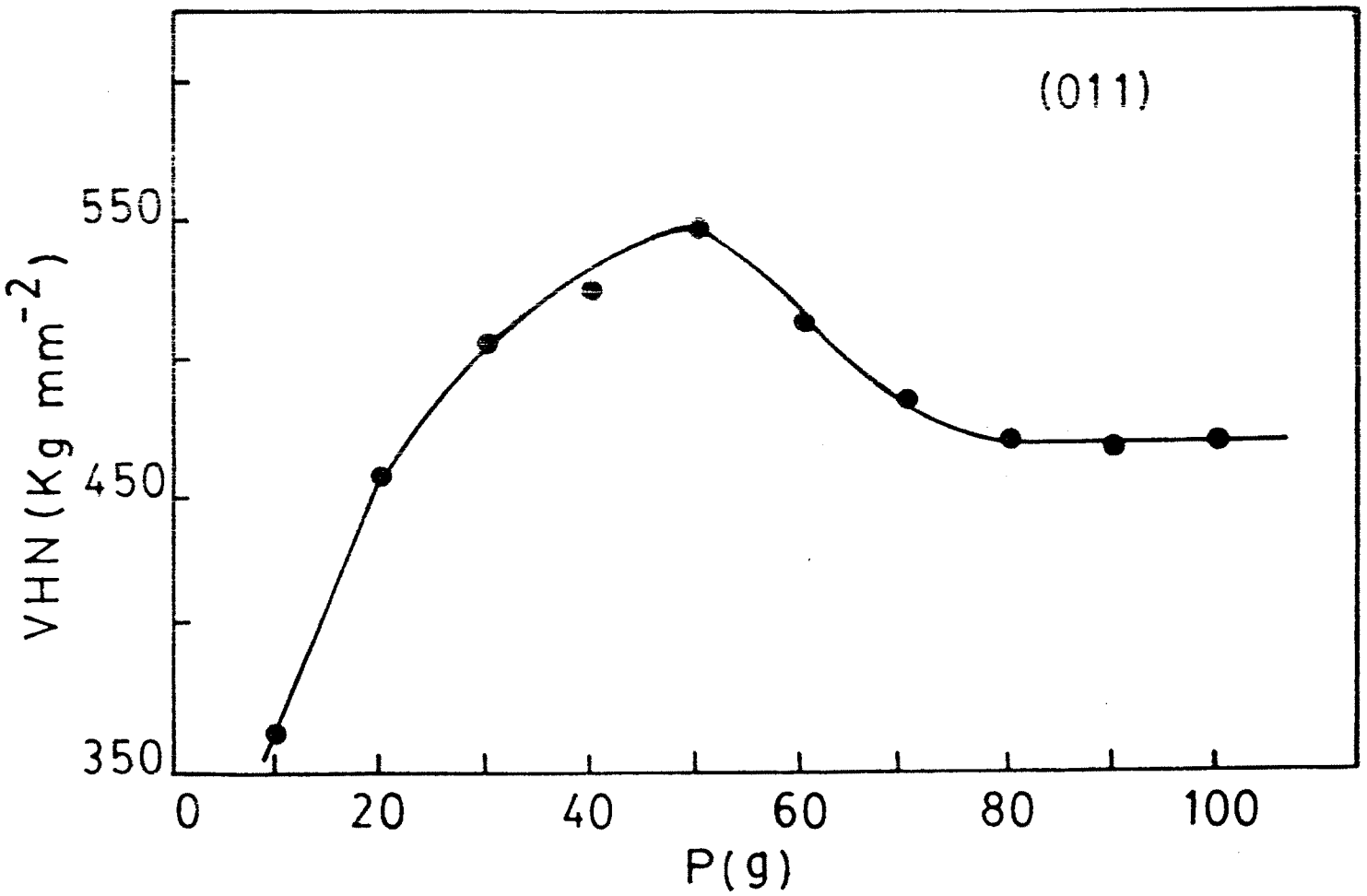

Fig. 7.2(a) Graphical variation of VHN with load for the as-grown (011) plane.

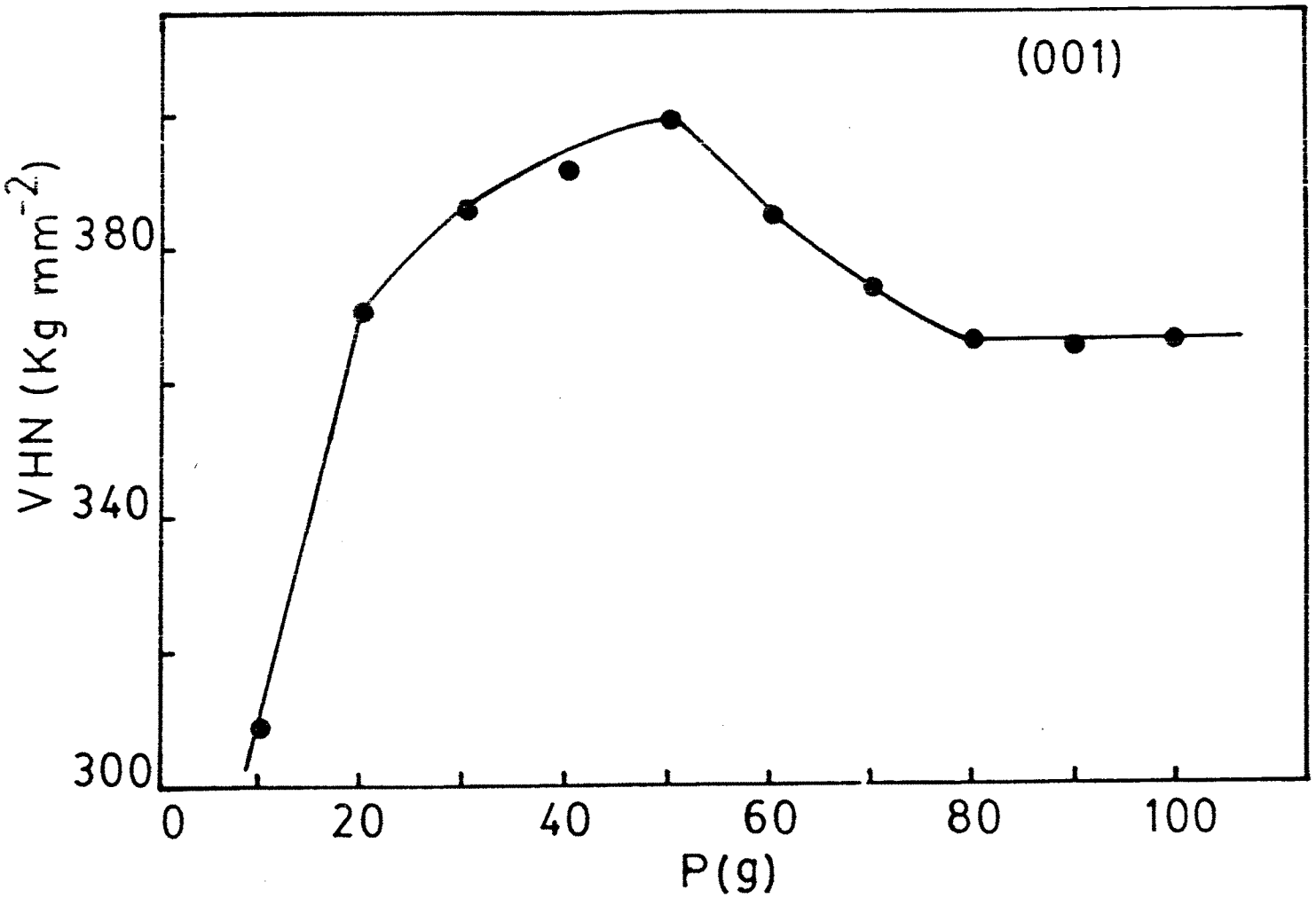

Fig. 7.2(b) Graphical variation of VHN with load for the cleaved (001) plane.

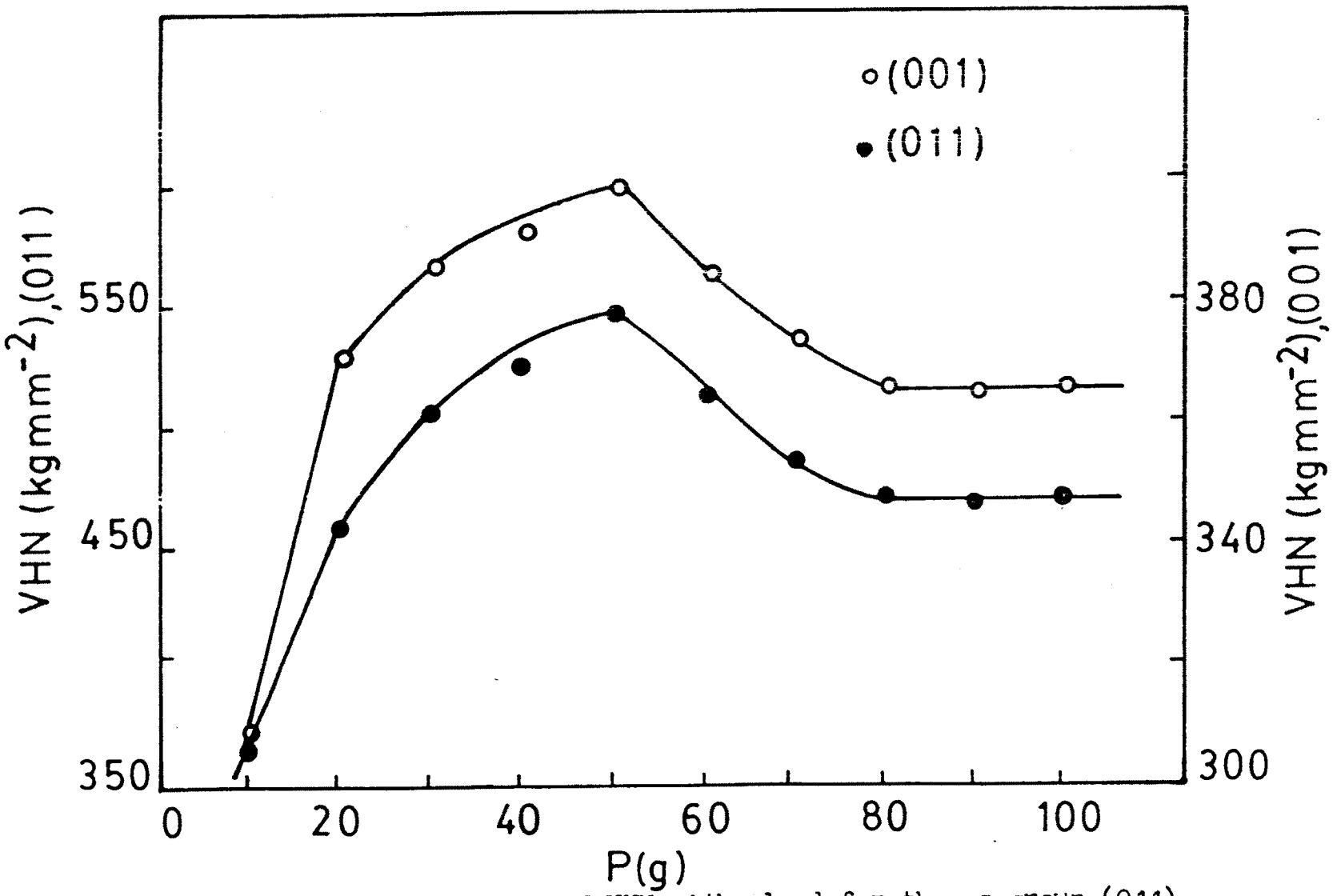

Fig. 7.3 Graphical variation of VHN with load for the as-grown (011) and cleaved (001) planes.

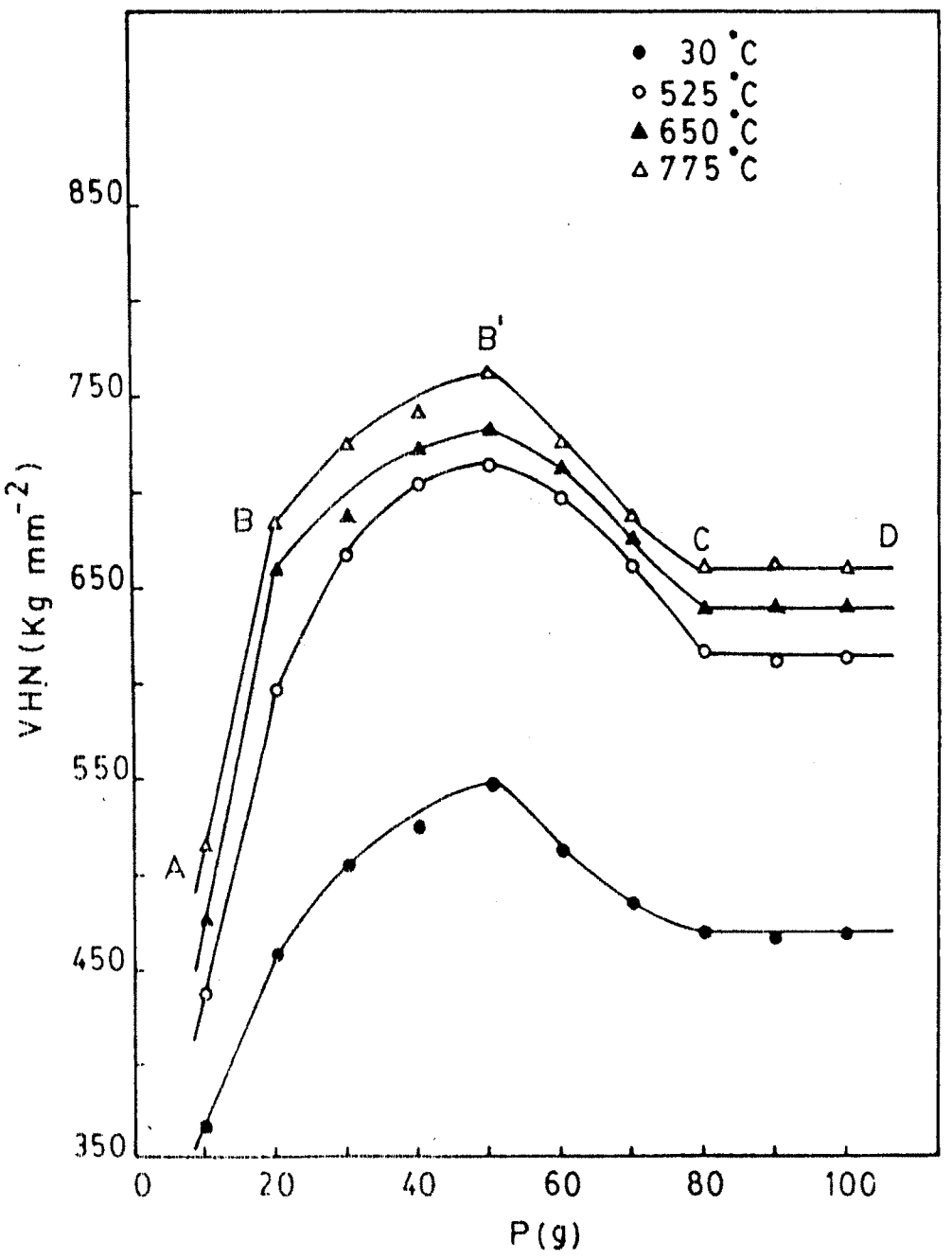

Fig. 7.4 Graphical plot of VHN versus load at different quenching temperatures for the as-grown (011) plane.

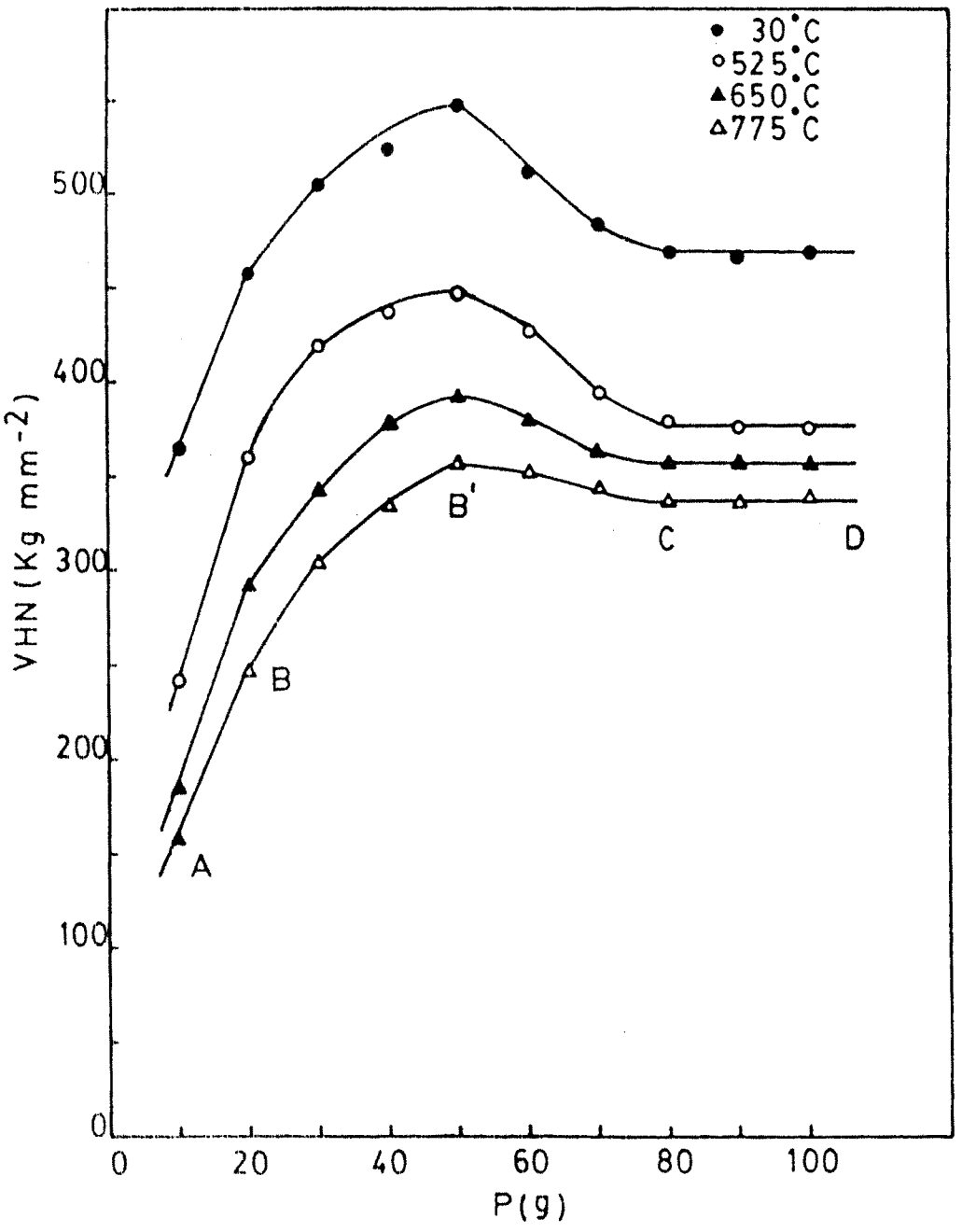

Fig. 7.5 Graphical plot of VHN versus load at different annealing temperatures for the as-grown (011) plane.

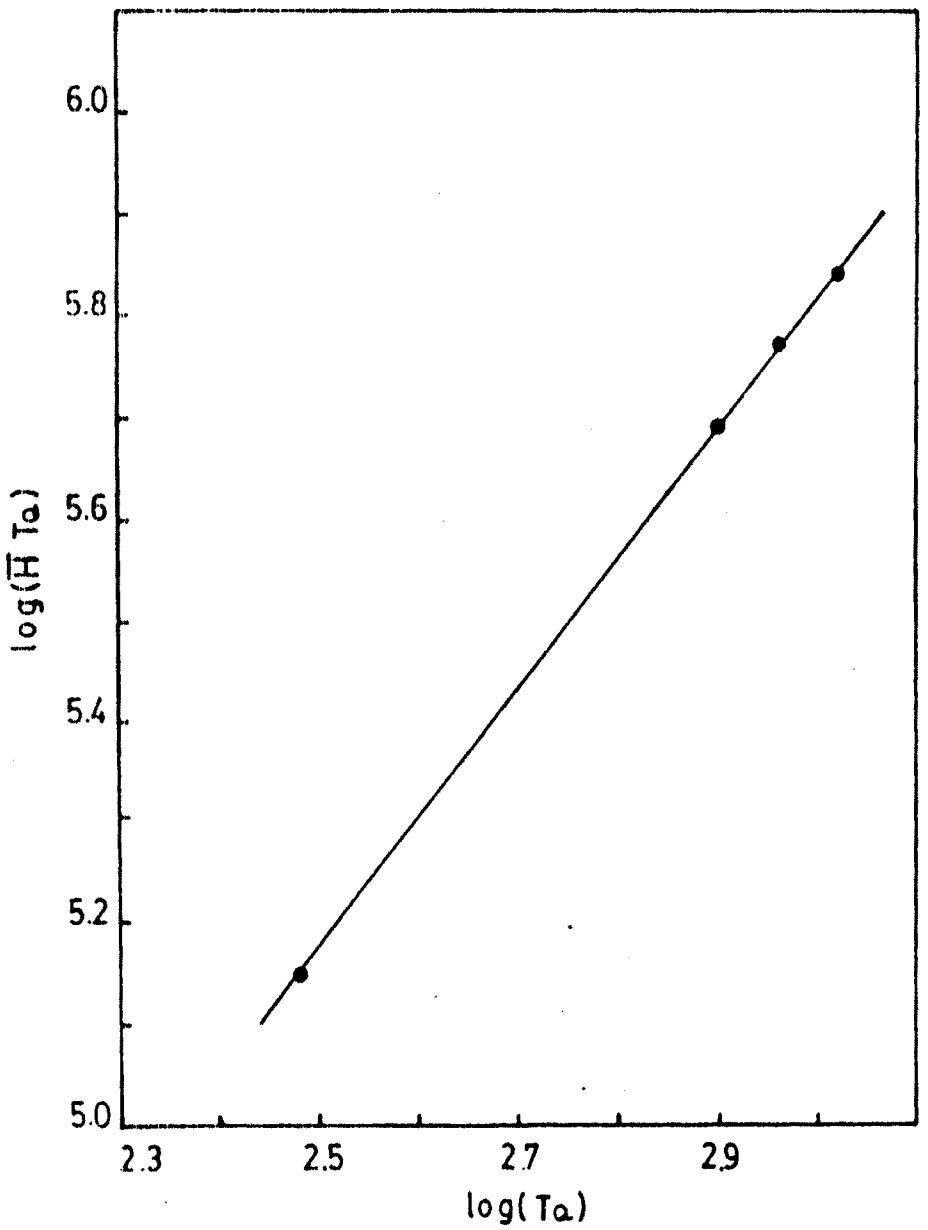

Fig. 7.6 log ($\bar{H}T_Q$) plotted against log (T_Q) for the as-grown (011) plane.

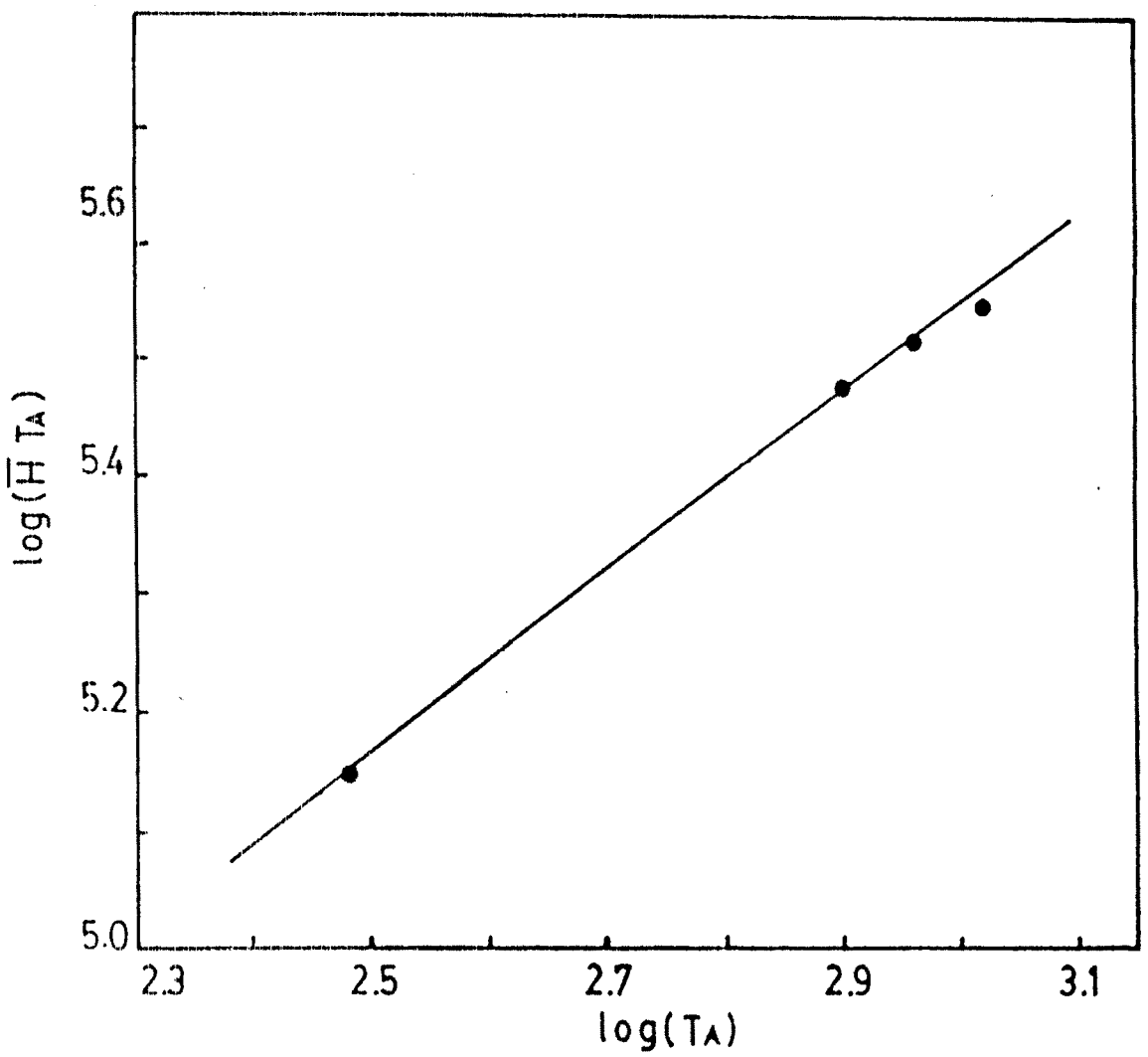

Fig. 7.7 log ($\bar{H}T_A$) plotted against log (T_A) for the as-grown (011) plane.

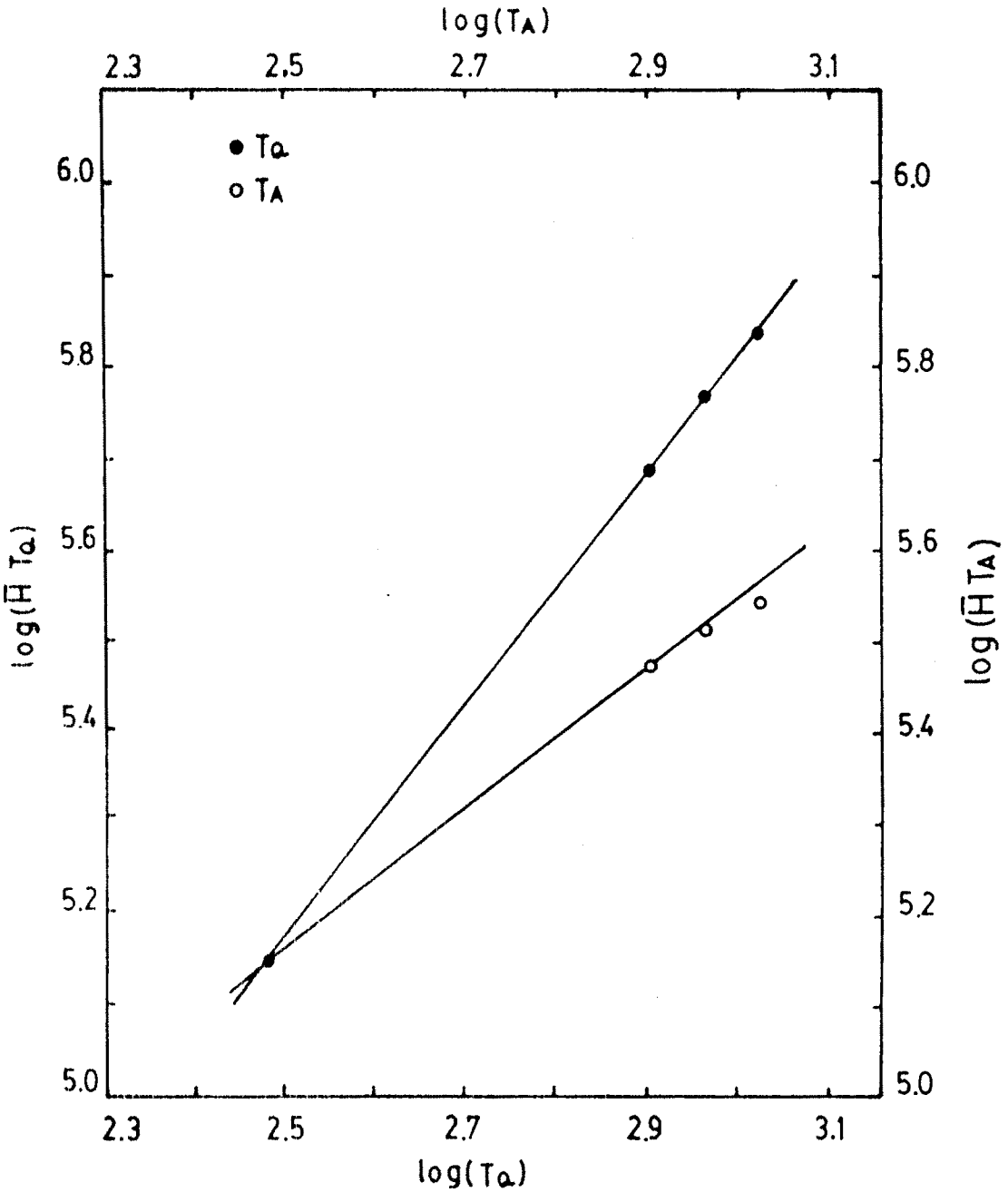

Fig. 7.8 Log ($\bar{H}T_Q$) plotted against log (T_Q) and log ($\bar{H}T_A$) plotted against log (T_A) for the as-grown (011) plane.

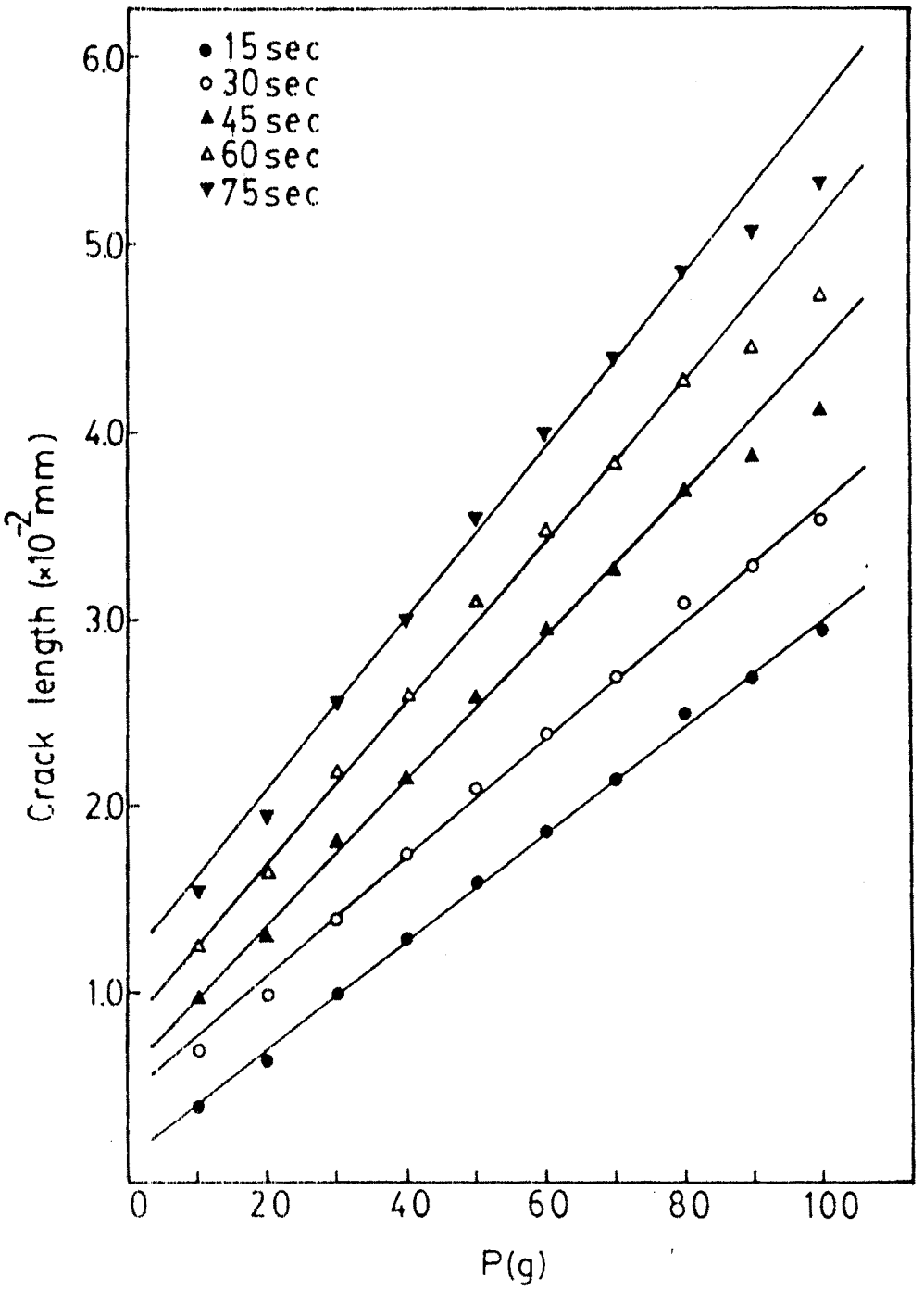

Fig. 7.9 The variation of crack length with the applied load at different indentation dwell periods.

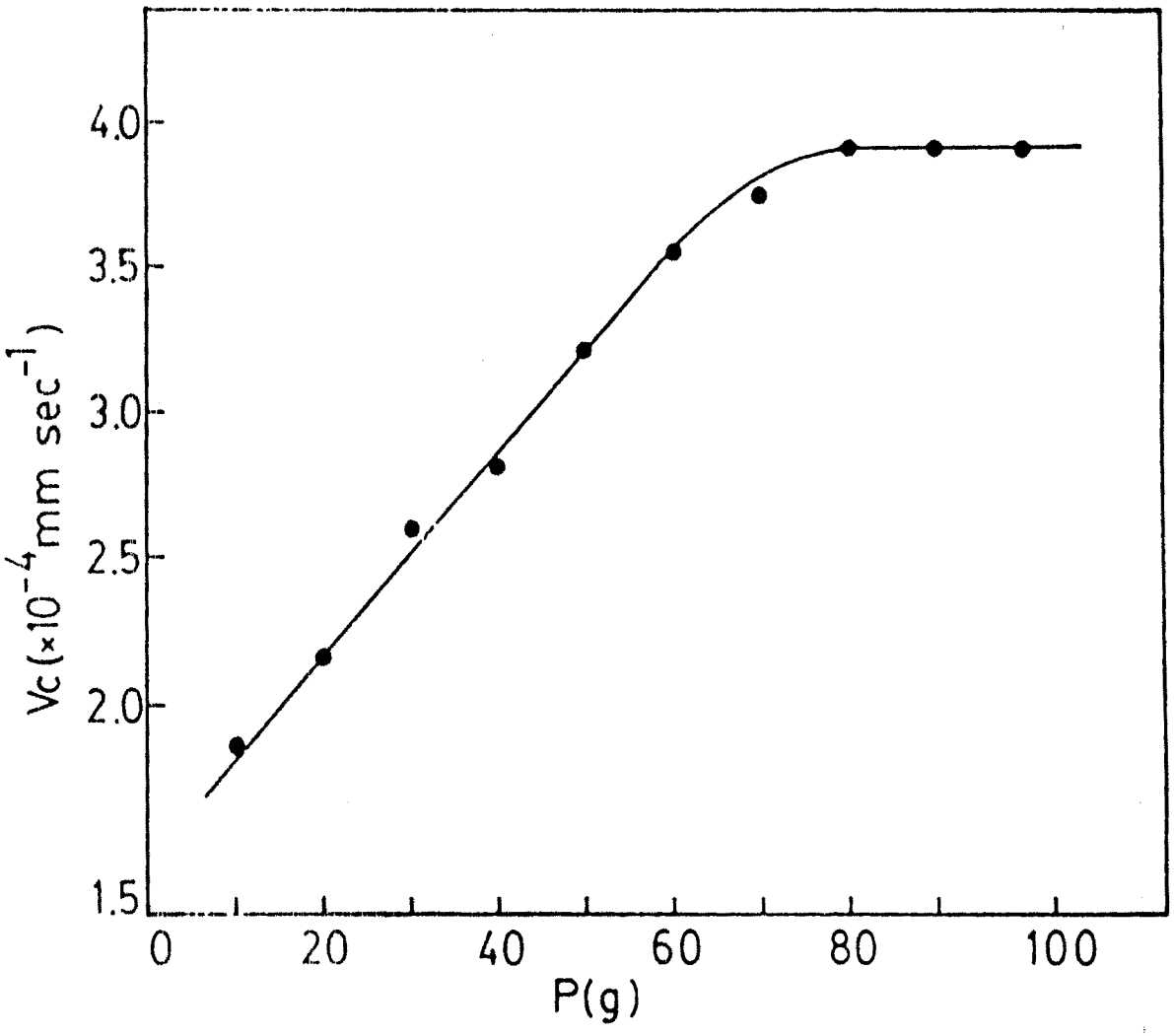

Fig.7.10 The variation of crack velocity with the applied load.

Fig. 7.11(a) Typical Vickers indentation mark on (011) face at 20 g load, exhibiting radical cracks, rc. X 690.

Fig. 7.11(b) The indentation mark on (011) face at 60 g load, exhibiting lateral cracks, lc, band of cracks, cz and crack free zone, cf. X 690.

Fig. 7.11(c) The indentation mark on (011) face at 100 g load, showing material chipping-off. X 690.

Typical Vickers indentation mark on (011) face at 20 g load, exhibiting radical cracks, rc. X 690.

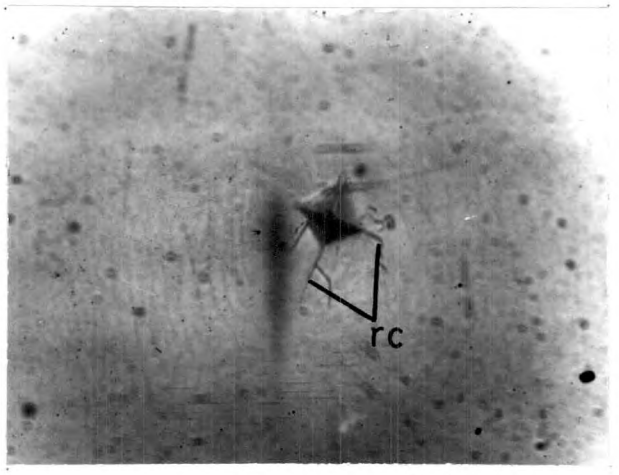

Fig. 7.11(a)

The indentation mark on (011) face at 60 g load, exhibiting lateral cracks, lc, band of cracks, cz and crack free zone, of . X 690.

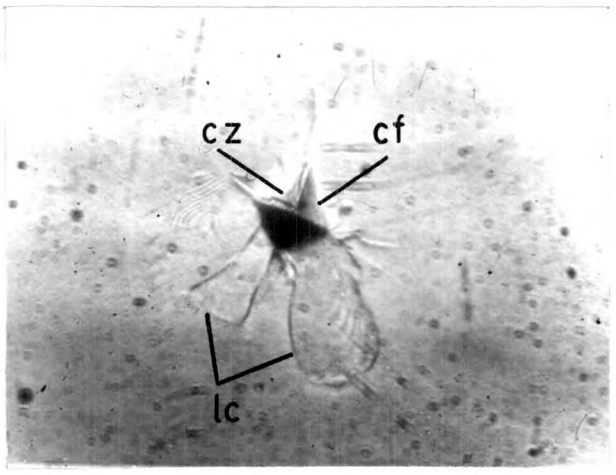

Fig. 7.11(b)

The indentation mark on (011) face at 100 g load, showing material chipping-off. X 690.

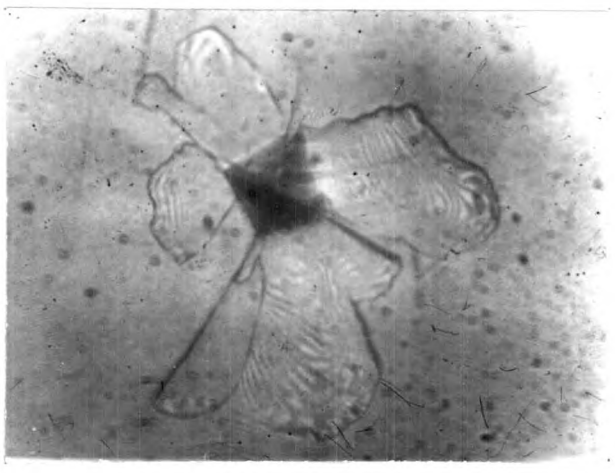

Fig. 7.11(c)